Supplementary Material

Molecular Crowding Creates Traffic Jams of Kinesin Motors On Microtubules

Cécile Leduc*[1,2], Kathrin Padberg-Gehle*[3], Vladimír Varga*[1,4], Dirk Helbing[5],

Stefan Diez[1,6,7] and Jonathon Howard[1,7]

1: Max Planck Institute of Molecular Cell Biology and Genetics, Pfotenhauerstraße 108, 01307 Dresden, Germany

2: Laboratoire Photonique Numérique et Nanosciences, Institut d'Optique Graduate School, Université de Bordeaux, CNRS, 351 cours de la libération, 33405 Talence, France

3: Technische Universität Dresden, Fachrichtung Mathematik, Institut für Wissenschaftliches Rechnen, 01062 Dresden, Germany

4: William Dunn School of Pathology, University of Oxford, South Parks Road, Oxford - OX1 3RE, UK

5: ETH Zürich, Clausiusstraße 50, 8092 Zürich, Switzerland

6: Technische Universität Dresden, B CUBE, Arnoldstraße 18, 01307 Dresden, Germany

7: corresponding authors: diez@bcube-dresden.de, howard@mpi-cbg.de

* equal contributions

Supplementary Table 1: List of parameters used in the simulations and the theoretical model

Symbol	Values [units]	Description
v_0	50 [nm/s]	free motor speed
d	8 [nm]	length of lattice site / dimer
L	[µm]	microtubule length
N	$N = L/d$	number of lattice sites / dimers
Δt	$\Delta t = d/v_0$ = 0.16 [s]	discrete time step
k_{on}	[$\mu m^{-1} \cdot s^{-1}$]	association rate (per unit length per unit time)
$\bar{k}_{\mathrm{on}}$	$\bar{k}_{\mathrm{on}} = k_{\mathrm{on}} d \Delta t = k_{\mathrm{on}} d^2 / v_0$	normalized association rate (nondimensional)
k_{off}	[s^{-1}]	lattice dissociation rate (per unit time)
$\bar{k}_{\mathrm{off}}$	$\bar{k}_{\mathrm{off}} = k_{\mathrm{off}} \Delta t$	normalized lattice dissociation rate (nondimensional)
k_{end}	[s^{-1}]	end dissociation rate (per unit time)
$\bar{k}_{\mathrm{end}}$	$\bar{k}_{\mathrm{end}} = k_{\mathrm{end}} \Delta t$	normalized end dissociation rate (nondimensional)
K	$K = \bar{k}_{\mathrm{on}} / \bar{k}_{\mathrm{off}}$	Langmuir constant (nondimensional)
$\bar{\rho}_s$	$\bar{\rho}_s = \frac{K}{1+K} = \frac{\bar{k}_{\mathrm{on}}}{\bar{k}_{\mathrm{on}} + \bar{k}_{\mathrm{off}}}$	Langmuir density level (nondimensional)
ρ	[d^{-1}]	motor density
ρ_{max}	[d^{-1}]	maximum motor density
$\bar{\rho}$	$\bar{\rho} = \rho / \rho_{max}$	normalized motor density (nondimensional)
v	$v(\rho) = v_0 (1 - \frac{\rho}{\rho_{max}})$ [nm/s]	motor speed
$\bar{v}$	$\bar{v}(\bar{\rho}) = 1 - \bar{\rho}$	normalized motor speed (nondimensional)

Methods

Protein assays: The 6xHis-Kip3-mCherry construct was created by exchanging the coding region of EGFP in 6xHis-Kip3-EGFP (1) by that of mCherry. Kip3 motors were expressed and purified as described previously for 6xHis-Kip3-EGFP (1). Microtubules (ratio of biotinylated to non-biotinylated tubulin 1:30) were polymerized in GMPCPP, further stabilized by 10 µM taxol (2), and bound to the surface of a flow chamber with anti-biotin antibodies (3). Flow chambers were constructed as described previously, with depth of 400 µm to minimize motor depletion out of solution (1). Assays were performed in BRB80 buffer (80 mM PIPES/KOH pH 6.9, 1 mM $MgCl_2$, 1 mM EGTA), supplemented with KCl (30 mM, 75 mM, 110 mM or 200 mM), ATP (1 mM Mg-ATP) and antifade (1% β-mercaptoethanol, 40 mM glucose, 40 µg/ml glucose oxidase, 16 µg/ml catalase) as described in reference (1). Both mCherry and EGFP fluorophores we excited with a 488 nm laser (Argon, Coherent) using TIRF microscopy. The bleedthrough from the red channel to the green channel was not detectable, and from the green channel to the red channel was negligible due to the low concentration of EGFP-labeled motors. Images were recorded on an EM-CCD (iXon-DV 897, Andor, Belfast, UK) camera with image acquisition every 1 to 20 s. Kymographs were generated and analyzed using Metamorph software (Molecular Devices Corporation, Sunnyvale, CA). Single-molecules were tracked by FIESTA software (4) written in MATLAB. Curves were fit using Igor (Wavemetrics, Lake Oswego, OR, USA). Uncertainties in calculated motor velocities (~20% of the mean) and densities were mainly due to the limited spatial resolution of our setup and the spatially non-uniform excitation in the TIRF microscope, respectively.

Kip3-mCherry: The properties of Kip3-mCherry in BRB80 supplemented with 110 mM KCl were very similar to those of Kip3-EGFP (2): the speed of single molecules was 53 ± 5 nm/s (mean ± SD, *n* = 52), the processivity was 13 ± 3 µm (mean ± SEM, *n* = 16 detachments), the end residency time in single-molecule conditions was 59 ± 35 s, mean ± SD, *n* = 37).

Simulations: The motor dynamics on a microtubule was modeled by a simple driven lattice gas cellular automaton based on the theoretical model by Parmeggiani et al. (5). Molecular motors were represented by particles and the microtubule by a one-dimensional discrete lattice with N grid cells (= attachment sites), where each site corresponds to a tubulin dimer of d = 8 nm. Assuming a free motor speed v_0 = 50 nm/s we set $\Delta t = d/v_0$ = 0.16 s.

The dynamic rules of the stochastic process were as follows:

(a) At the site i = 1, ..., N-1, a particle can jump to site i+1 if unoccupied with probability $v_0 \Delta t/d = 1$;

(b) at the site i = N (i.e. the microtubule end) a particle can leave the lattice with the normalized end dissociation rate $\bar{k}_{\mathrm{end}} = k_{\mathrm{end}}\Delta t$, where k_{end} is the end dissociation rate (s^{-1}). $\bar{k}_{\mathrm{end}}$ varies between 0 and 1.

(c) at the site i = 1, ..., N-1, a particle can leave the lattice with the normalized lattice dissociation rate $\bar{k}_{\mathrm{off}} = k_{\mathrm{off}}\Delta t$ (where $\bar{k}_{\mathrm{off}} \leq \bar{k}_{\mathrm{end}}$), where k_{off} is the lattice dissociation rate (s^{-1}).

(d) at the site i = 1, ..., N-1, a particle can enter the lattice with landing rate $\bar{k}_{\mathrm{on}} = k_{\mathrm{on}} d\Delta t = k_{\mathrm{on}} d^2/v_0$, where k_{on} is the association rate (per unit length per unit time).

Processes (a) and (b) correspond to a totally asymmetric simple exclusion process with open boundaries, while processes (c) and (d) constitute a Langmuir kinetics.

Experiments suggest that landing rates are close to $\overline{k}_{\mathrm{on}} = C \cdot 10^{-4}$, where C corresponds to the Kip3 concentration in solution (in [nM]). The constant k_0 = 10^{-4}, such as $\overline{k}_{\mathrm{on}} = k_0 C$, was however allowed to be changed up to 25% in order to fit experiments with the same concentration C but done on different days. This flexibility was given to circumvent unavoidable experimental errors on the evaluation of C. We also used the notation $\overline{k}_{\mathrm{on}} = x/\mathrm{N}$, where x < 0.5 corresponds to cases with low landing rates or short microtubules, and x > 0.5 to high landing rate regimes or long microtubules. This notation allows a simple comparison with the analytical and numerical results in Parmeggiani et al. (5). We applied Monte-Carlo simulations with a random-sequential update (5), which mimics the transitions as Poisson processes. Both, time and sample averages were evaluated to obtain the stationary profiles of the motor density. They coincide for both averaging procedures (using 10^5 time averages/samples). The temporary evolution of the density profiles was obtained over 10^4 sample averages, the simulated kymographs in Figures 4 and 5 over 1000 sample averages. The computations as well as the visualization of the results were carried out in MATLAB. A list of the parameters used in the simulations is presented in Supplementary Table 1.

For the computation of the phase diagrams we considered a prototypical microtubule of length 10 µm (i.e. N = 1250) and different fixed values of the affinity $K = \overline{k}_{\mathrm{on}} / \overline{k}_{\mathrm{off}}$. We varied the end dissociation rate $\overline{k}_{\mathrm{end}}$ from 0 to 1 in steps of 0.01 and computed the stationary density profiles (10^4 time averages). For each K, we analyzed the profiles in particular with respect to (i) the maximum $\overline{k}_{\mathrm{end}}$ to observe jams (boundary between domains b and c in Figure 4 and 5 in the main text) and (ii) the existence of end-spikes in the low density (LD) regime (boundary between domains a and b in Figure 4 and 5 in the main text). For (i) we determined the number n of lattice sites x with $\overline{\rho}(x) > 0.5$, where $\overline{\rho}$ is the normalized motor density ρ/ρ_{max}, ρ_{max} being the maximal density along the lattice. The data points ($\overline{k}_{\mathrm{end}}$, $n(\overline{k}_{\mathrm{end}})$) were fit by a high degree polynomial (degree five to nine). The point of maximum curvature of the resulting curve (i.e. maximum of the second derivative) defined the critical parameter for jam formation (see Figure S-I below). At this point, the jam growth increased rapidly if $\overline{k}_{\mathrm{end}}$ was decreased. For (ii) we considered the average density close to the microtubule-end $\overline{\rho}(L^-)$, if L is the length of the microtubule. An end-spike was observed if $(1 - \overline{k}_{\mathrm{end}}) > \overline{\rho}(L^-)$.

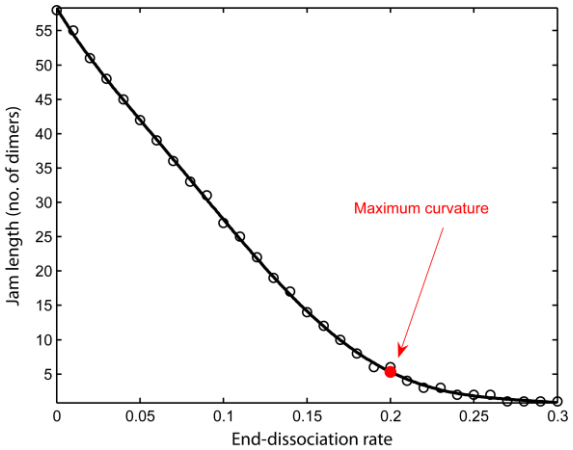

Figure S-I: Determination of the critical $\overline{k}_{\mathrm{end}}$ for jam formation. The point of maximum curvature in the polynomial fit of jam length n vs. $\overline{k}_{\mathrm{end}}$ determines the critical parameter where jam formation is initiated. In this case $\overline{k}_{\mathrm{on}} = 8$ x $10^{-4} = 1/N$ (N = 1250) and K = 0.25 (i.e. $\overline{\rho}_{\mathrm{s}} = K/(1+K) = \overline{k}_{\mathrm{on}} / (\overline{k}_{\mathrm{on}} + \overline{k}_{\mathrm{off}}) = 0.2$). The critical $\overline{k}_{\mathrm{end}}$ is 0.2 and matches the theoretical value for high association rates.

Theoretical model

Flux equation: Balancing the fluxes in the figure S-II leads to a conservation equation:

$$\frac{\partial \rho}{\partial t}(x,t) = -\frac{\partial}{\partial x}[\rho(x,t)v(\rho)] + k_{\text{on}}\left(1 - \frac{\rho(x,t)}{\rho_{\max}}\right) - k_{\text{off}}\rho(x,t) \qquad (1)$$

where k_{on} is the lattice-association rate (per unit length per unit time), k_{off} the lattice-dissociation rate (per unit time), ρ the motor density, ρ_{max} the maximum density of motors and v, the motor speed. We assume that k_{on} and k_{off} are constants and that *v* depends only on density. ρ_{max} , the maximum density of motors, is assumed to be equal to 1/*d* (*d* is the tubulin dimer length of 8 nm), and this corresponds to full occupancy of the lattice. The left-hand boundary condition is $\rho(0,t) = 0$. At the right-hand boundary, when dissociation is limiting, $v(L) = k_{end}d$ where k_{end} is the end-dissociation rate and L is the microtubule length. We previously showed that $k_{end}(\rho)$ increases with density (2), but we will assume that it has a constant value (the high-density limit) in the present work.

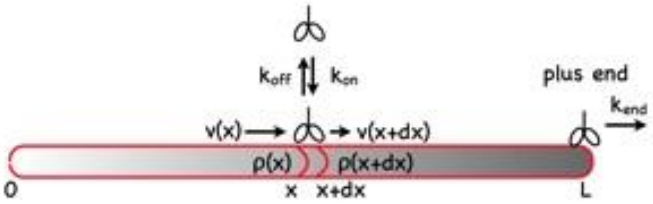

Figure S-II: Balance of Fluxes

Provided that the dissociation from the plus end can keep up with the flux to the end, the right-hand boundary can be considered open. However, if the dissociation cannot keep up with the flux to the end, then equality holds, and the equation has two boundary conditions. In general, a first-order differential equation can only satisfy one boundary condition; thus, the system is overdetermined: if motor dissociation from the end is limiting, there will generally be a discontinuity where the solutions from the two microtubule ends meet.

We assume that the speed decreases linearly with density up to the Langmuir density level as observed experimentally: $v(\rho) = v_0$ (1 - ρ / ρ_{max}), where v_0 is the maximum speed (at zero density). Therefore the normalize speed $\bar{v} = v/v_0 = 1 - \bar{\rho}$, where $\bar{\rho} = \rho/\rho_{max}$ is the normalized density.
In the steady state equation 1 implies:

$$\frac{d\bar{\rho}\bar{v}}{d\bar{x}} = \frac{d}{d\bar{x}}[\bar{\rho}(1-\bar{\rho})] = \bar{k}_{\text{on}}(1-\bar{\rho}) - \bar{k}_{\text{off}}\bar{\rho} \qquad (2)$$

Then, $$\frac{d\bar{\rho}}{d\bar{x}} = \bar{k}_{\text{on}}\frac{1-\bar{\rho}/\bar{\rho}_s}{1-2\bar{\rho}} \qquad (3)$$

where $\bar{\rho}_s = K/(1+K) = \bar{k}_{\text{on}}/(\bar{k}_{\text{on}}+\bar{k}_{\text{off}})$.
When the density reaches ½, the denominator goes to zero and this corresponds to an abrupt density change, which is the characteristic for traffic jams.

Jam formation: The condition for the creation of a traffic jam nucleated at the plus end of the microtubule (a bottleneck-induced jam) is that the arriving flux of motors to the microtubule end exceeds the end-dissociation flux. In other words, these jams are caused by bottlenecks just like in car

traffic. Using normalized parameters, and knowing that the density at the microtubule end is: $\overline{\rho}(L) = 1 - \overline{k}_{\mathrm{end}}$, the end-dissociation flux is: $\overline{\rho}(L)\overline{k}_{\mathrm{end}} = \left(1 - \overline{k}_{\mathrm{end}}\right)\overline{k}_{\mathrm{end}}$.
Assuming a linear relationship between speed and density, as shown experimentally, the flux of arriving motors at microtubule end is : $\overline{\rho}(L^{-})\overline{v}(L^{-}) = \overline{\rho}(L^{-})\left(1 - \overline{\rho}(L^{-})\right)$, where L^{-} represents the distance from the minus end to a position close to the plus end.

The equation defining the bottleneck-induced jams is therefore

$$(1 - \overline{k}_{\mathrm{end}})\overline{k}_{\mathrm{end}} < \overline{\rho}(L^{-})\left(1 - \overline{\rho}(L^{-})\right) \qquad (4)$$

At low association-rate ($\overline{k}_{\mathrm{on}} \leq 0.5/M$), this equation defines the transition between domain b and c in Figure 4 (central panel) in the main text. At high association-rate ($\overline{k}_{\mathrm{on}} \geq 0.5/M$), it is possible to associate the motor density close to the microtubule end with the Langmuir density $\overline{\rho}_{\mathrm{s}}$. The equation defining the bottleneck-induced jams becomes:

$$(1 - \overline{k}_{\mathrm{end}})\overline{k}_{\mathrm{end}} \leq \overline{\rho}_{\mathrm{s}}\left(1 - \overline{\rho}_{\mathrm{s}}\right) \qquad (5).$$

For $\overline{k}_{\mathrm{end}} \leq 0.5$ and $\overline{\rho}_{\mathrm{s}} \leq 0.5$, this condition implies that $\overline{k}_{\mathrm{end}} \leq \overline{\rho}_{\mathrm{s}}$, which corresponds to domain c in the phase diagram shown in Figure 5 in the main text.
For $\overline{\rho}_{\mathrm{s}} \geq 0.5$ and $\overline{k}_{\mathrm{end}} \leq 0.5$, density-induced jams are formed at the same time as bottleneck-induced jams (domain d in phase diagram Figure 5 in the main text).
For $\overline{\rho}_{\mathrm{s}} \geq 0.5$ and $\overline{k}_{\mathrm{end}} \geq 0.5$, only density-induced jams occur (domain e in phase diagram Figure 5 in the main text). Density-induced jams are caused by a very high motor density on the lattice due to high landing rates. They are also known as phantom jams in the traffic science community.

Jam velocity: In the reference system of the moving jam (see Figure S-III):

- the motor speed in the low density (LD) region is: $v_{LD} + v_{\mathrm{jam}}$
- the motor speed in the high density (HD) region is: $v_{HD} + v_{\mathrm{jam}}$

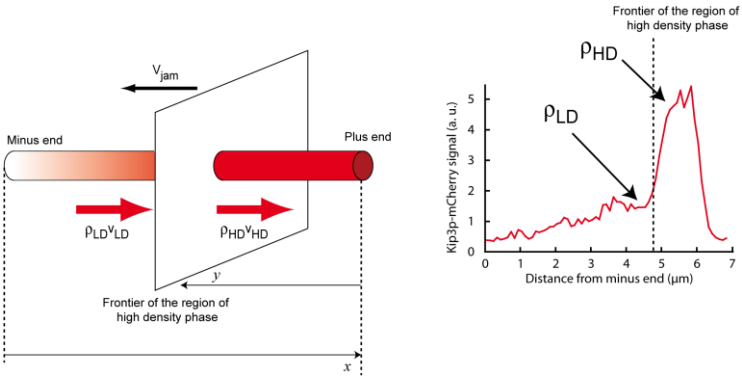

Figure S-III: Definition of parameters

All the velocities are positive, signs have been chosen accordingly. Let v_0 be the speed of motors in the absence of neighbors (corresponding to single-molecule conditions). Then, the flux balance at the frontier of the traffic jams gives:

$$\rho_{LD}\left(v_{LD} + v_{\mathrm{jam}}\right) = \rho_{HD}\left(v_{HD} + v_{\mathrm{jam}}\right) \qquad (6)$$

Let *y* be the length of the traffic jam (see Figure S-III):

$$v_{\text{jam}} = dy/dt \tag{7}$$

Then,

$$\frac{dy}{dt} = \frac{1}{\rho_{HD} - \rho_{LD}} \left(\rho_{LD} v_{LD} - \rho_{HD} v_{HD}\right) \tag{8}$$

If we assume that $\rho_{LD} << \rho_{HD}$ and $v_{LD} = v_{0,}$ the antenna model (2), which assumes a uniform binding, constant velocity and very high processivity of motors, gives:

$$\rho_{LD} = \frac{k_{\text{on}}}{v_0} (L - y) \tag{9}$$

where L is the microtubule length and k_{on} the landing rate.
Using (8) and (9), we obtain:

$$\frac{dy}{dt} + \frac{k_{\text{on}}}{\rho_{HD}} y = \frac{k_{\text{on}}}{\rho_{HD}} L - v_{HD} \tag{10}$$

Integration of differential equation 10 gives:

$$y(t) = \left(L - v_{HD} \frac{\rho_{HD}}{k_{\text{on}}}\right) \left(1 - \exp\left(-\frac{k_{\text{on}}}{\rho_{HD}} t\right)\right) \tag{11}$$

Equation 11 was used to fit the traffic jam growth curves in Figure 3 in the main text. This equation holds when the antenna model can be applied, which means when the motor lattice dissociation rate can be neglected (k_{off} close to 0) and when the association rate is low enough in order that saturation effects do not appear in the LD region ($\rho_{LD} << \rho_{HD}$). This corresponds to domain c in the phase diagram of Figure 4 in the main text and to the cases, which could be fit experimentally (Fig. 2 in the main text and Fig. S4).

Supplementary Figures

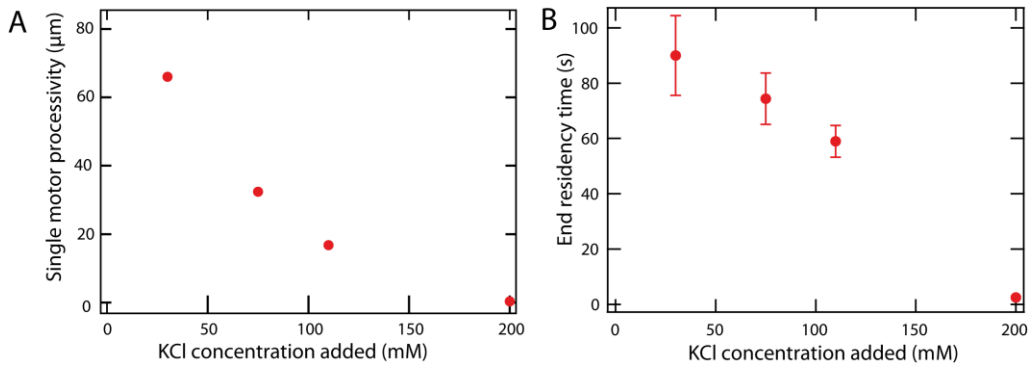

Figure S1: Experimental average processivity of single Kip3 motors (A) and their average end residency time (B) as function of the KCl concentration. Data were acquired at low motor concentration (< 0.05 nM Kip3-EGFP, no Kip3-mCherry), to keep the motor density close to zero and thereby to minimize effects of interactions between motors. The motor processivity in (A), calculated as the average travel length before detachment (the number of motor detachments was n=1, 8, 10, and 203 for the salt concentrations of 30, 75, 110 and 200 mM KCl respectively), divided by v_0 (free motor speed), yields the inverse of the lattice detachment rate. The inverse of the end residency time in (B) is the motor end-dissociation rate. Both the lattice dissociation rate and end dissociation rate increase with increasing concentration of KCl. Note that these rates also increase with increasing density of Kip3 on the lattice (2). Error bars in (B) denote S.E.M.

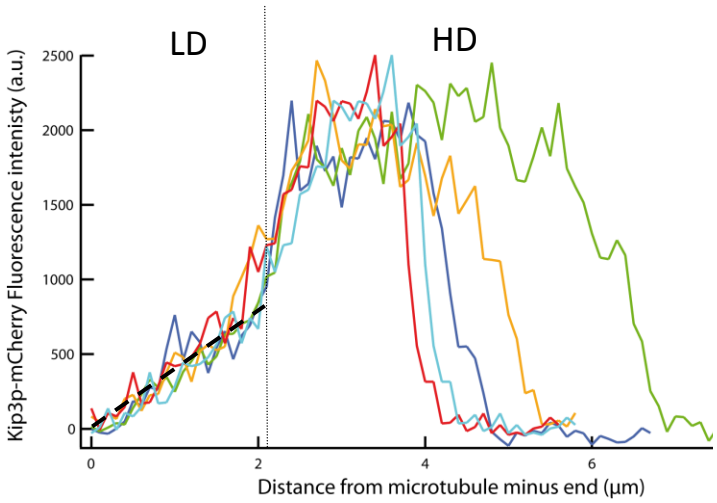

Figure S2: Experimental motor densities on microtubules of various lengths after steady state was reached. In the experiments, 3.2 nM Kip3-mCherry was present in solution. The intensity in the HD region was independent of the microtubule length. Note that the jams stopped at the same distance from the minus-end for all the microtubules (dotted line). This is a consequence of the antenna model (2): The jam growth stops when – at the jam boundary – the incoming flux from the LD region balances the flux in the HD region. Because all microtubules have the same density gradient in the LD region (dashed line, due to the antenna model), the fluxes coming from the LD regions into the HD regions are equal for all microtubules.

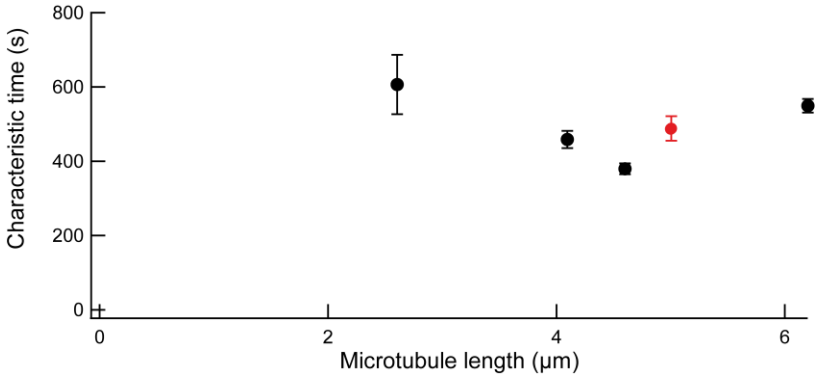

Figure S3: Experimental characteristic time associated with the exponential approach of the jam length to steady state as function of microtubule length (same data as in Fig. 2C in the main text). Error bars denote the estimated SD of the fit coefficients. The red point corresponds to the microtubule shown in Fig. 2A and C.

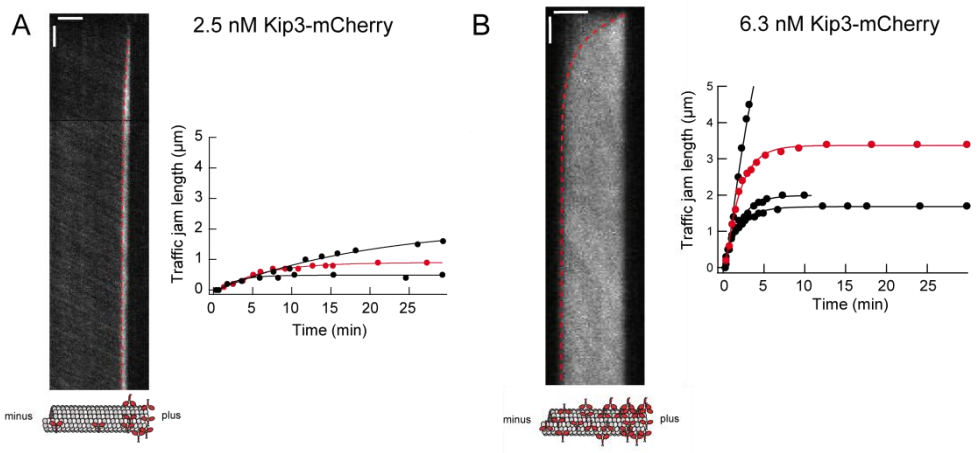

Figure S4: Experimental kinetics of traffic jam growth for Kip3 motor concentrations of 2.5 nM in (A) and 6.3 nM in (B). Kymographs show an example of jam growth at given Kip3p concentration. The red dashed line denotes the position of the frontier of the HD region and represent the fit using equation 11. The graphs show the traffic jam length (i. e. the distance of the frontier of the HD region from the plus end) in time for several microtubules of different lengths (3.4, 17.1, and 30.5 µm from bottom to top in (A) and 1.9, 2.2, 3.6, 4.9 µm (B)). The curves were fit using equation 11. The red curves correspond to the jam depicted in the kymograph. Bars, 2 µm (horizontal) and 2 min (vertical).

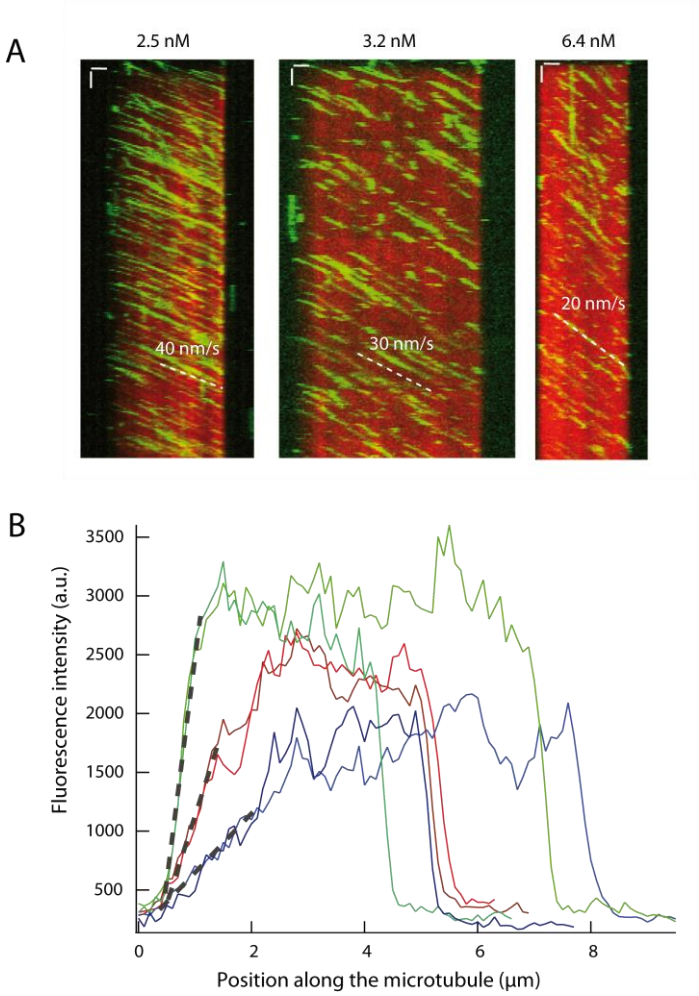

Figure S5: Experimental Kip3 velocities and densities at 110 mM KCl. (A) Dual-color kymographs showing the motor density in red (Kip3-mCherry, 2.5, 3.2 and 6.4 nM in solution) and the behavior of individual motors in green (Kip3-EGFP, < 0.05 nM in solution) in the presence of 110 mM KCl. Bars, 1 µm (horizontal) and 1 min (vertical). The motor density on the microtubule lattice in the HD region increases with Kip3-mCherry concentration (the intensity is scaled identically in each kymograph). This increase in motor density leads to a decrease in motor speed (dashed lines). (B) Motor-density profiles for different Kip3-mCherry concentrations (2.5 nM, blue curves; 3.2 nM, red curves and 6.4 nM Kip3, green curves; two microtubules for each condition) in the presence of 110 mM KCl. For a given Kip3 concentration a gradient of identical slope (dashed lines) is present on various microtubules, as observed previously (2). The slope increases with Kip3 concentration as does the plateau of the HD region. At the highest concentration, the slope of the density gradient (LD region) is indistinguishable from the slope of the density-induced jam front.

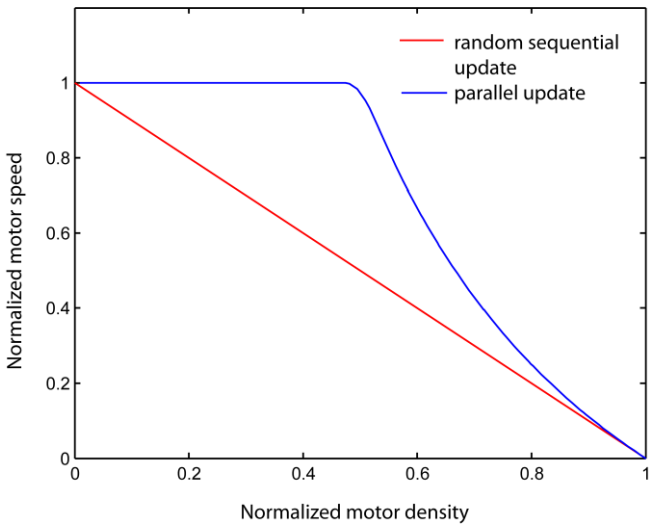

Figure S6: Simulated results for the speed-density relationship considering the motors as random steppers (memory-less behavior, implemented by a random sequential update, red curve) or as partially synchronized steppers (implemented by a parallel updating procedure, blue curve). Assuming a memory-less behavior, the speed decays linearly with density, as observed in our experiments. If motors can fully synchronize to a train-like motion, the speed will become independent of density. In the case of partial synchronization shown here, this applies for small densities; for normalized densities > 0.5 the speed decays polynomially with density.

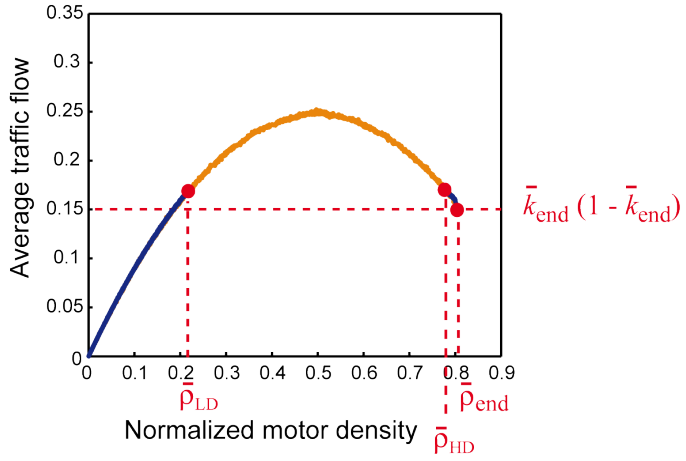

Figure S7: Simulated relationship between the traffic flow and normalized motor density using the parameters $\bar{k}_{on}$ = 2 x 10^{-4} = 0.25/*N*, $\bar{\rho}_s = 0.91$ and $\bar{k}_{end}$ = 0.2 (equivalent to 2 nM Kip3) (blue points); $\bar{k}_{on}$= 8 x 10^{-4}= 1/*N* with *N* = 1250, $\bar{\rho}_s$ = 0.5 and $\bar{k}_{end}$ = 0.2 (equivalent to 8 nM Kip3) (orange points). This diagram is associated with the speed vs. normalized motor density Fig.3D (main text).

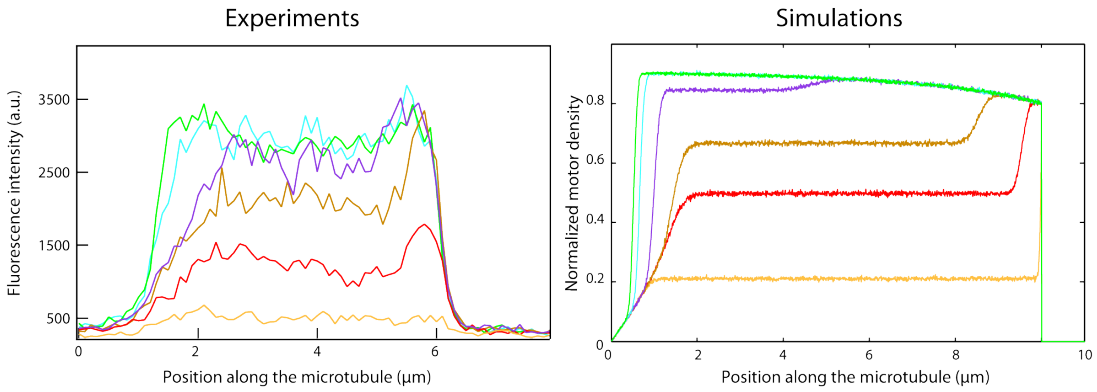

Figure S8: Experimental (left) and simulated (right) time evolution of the motor density on a given microtubule in domain d (Fig. 5 in the main text) . Experiments were performed with 6.4 nM Kip3 in the presence of 30 mM KCl. Kip3-mCherry intensities are plotted at 5 s (yellow curve), 25 s (red), 50s (brown), 75 s (purple), 150 s (light blue) and 200 s (light green) after addition of Kip3-mCherry to the microtubule. Comparison with simulation using $\bar{k}_{\mathrm{on}}$ = 1.6 x 10^{-3} = 2/N, $\bar{\rho}_{\mathrm{s}}$ = 0.91, $\bar{k}_{\mathrm{end}}$ = 0.2 (domain d), N = 1250. Density profiles plotted at 24 s (yellow curve), 72 s (red), 120 s (brown), 240 s (purple), 360 s (light blue) and 480 s (light green). We observe the formation of a density-induced jam along the lattice when the critical density 0.5 is reached and independently the formation of a bottleneck induced jam.

Movie S1. Formation of a traffic jam of Kip3 on a microtubule

Sequence of time-lapse images shows the formation of a traffic jam of Kip3 (mixture of 3.2 nM Kip3-mCherry and < 0.05 nM Kip3-EGFP) added to the microtubule at the beginning of the movie. The traffic jam is characterized by an abrupt increase in motor density (as apparent from the red Kip3-mCherry signal) and by an abrupt decrease in motor speed (as apparent from the green signal of individual Kip3-EGFP molecules). Both, red and green TIRF images, were recorded every 20 s and are displayed at 15 frames per second in the movie. Scale bar, 2 µm.

Bibliography

1. Varga V*, et al.* (2006) Yeast kinesin-8 depolymerizes microtubules in a length-dependent manner. *Nat Cell Biol* 8:957-962.
2. Varga V, Leduc C, Bormuth V, Diez S, & Howard J (2009) Kinesin-8 motors act cooperatively to mediate length-dependent microtubule depolymerization. *Cell* 138:1174-1183.
3. Fink G*, et al.* (2009) The mitotic kinesin-14 Ncd drives directional microtubule-microtubule sliding. *Nat Cell Biol* 11:717-723.
4. Ruhnow F, Zwicker D, & Diez S (2011) Tracking single particles and elongated filaments with nanometer precision. *Biophys J* 100:2820-2828.
5. Parmeggiani A, Franosch T, & Frey E (2003) Phase coexistence in driven one-dimensional transport. *Phys Rev Lett* 90:086601.